PHYSICAL REVIEW E **77**, 050901(R) (2008)

Mesoscale modeling of molecular machines: Cyclic dynamics and hydrodynamical fluctuations

Andrew Cressman,[1,*] Yuichi Togashi,[2,†] Alexander S. Mikhailov,[3,‡] and Raymond Kapral[1,§]
[1]*Chemical Physics Theory Group, Department of Chemistry, University of Toronto, Toronto, Ontario, Canada M5S 3H6*
[2]*Graduate School of Frontier Biosciences, Osaka University, 1-3 Yamadaoka, Suita, Osaka 565-0871, Japan*
[3]*Abteilung Physikalische Chemie, Fritz-Haber-Institut der Max-Planck-Gesellschaft, Faradayweg 4-6, 14195 Berlin, Germany*
(Received 25 January 2008; published 7 May 2008)

Proteins acting as molecular machines can undergo cyclic internal conformational motions that are coupled to ligand binding and dissociation events. In contrast to their macroscopic counterparts, nanomachines operate in a highly fluctuating environment, which influences their operation. To bridge the gap between detailed microscopic and simple phenomenological descriptions, a mesoscale approach, which combines an elastic network model of a machine with a particle-based mesoscale description of the solvent, is employed. The time scale of the cyclic hinge motions of the machine prototype is strongly affected by hydrodynamical coupling to the solvent.

DOI: 10.1103/PhysRevE.77.050901 PACS number(s): 87.10.Mn, 87.15.H−, 82.39.−k

Molecular machines, acting as motors, enzymes, or ion pumps, are involved in the function of biological cells [1,2] and are fundamental elements in applications in soft matter nanotechnology [3]. Their operation relies on conformational motions in proteins, with time scales typically ranging between milliseconds and seconds. Although structures of machine proteins are known, full molecular dynamics simulations of such slow internal motions are currently not feasible. Therefore, theoretical analysis of stochastic dynamics of molecular machines is often based on simple models that describe these complex biomolecules as single-coordinate ratchets or oscillators [4,5]. This approach has been successful in clarifying some principal aspects of machine operation [6], but the connection between simple phenomenological models and actual protein machines is often not evident. The gap between realistic microscopic models and simplified phenomenological approaches is an obstacle to the theoretical understanding of machine operation.

Mesoscale models, which can fill this gap, are already broadly used to describe polymer dynamics and protein folding [7]. In elastic network models, a protein is represented by a set of identical beads (coarse grained atomic groups) connected by identical elastic bonds; the pattern of connections is determined by the known equilibrium conformation of a given protein [8]. Remarkably, elastic network models can reproduce large-amplitude slow conformational motions in many proteins [9], including some aspects of nonlinear conformational relaxation [10,11].

Protein machines operate in molecular environments and solvent hydrodynamical effects play an important role in their dynamics. Solvent particles can be included in microscopic molecular dynamics simulations, but this is computationally challenging. In contrast, continuum hydrodynamical models cannot account for either molecular fluctuations or specific interactions. Coarse grained molecular dynamics schemes for the solvent can be used to incorporate both interactions and fluctuations [12].

In this paper, we show that mesoscale models, combining coarse grained descriptions for molecular machines and their solvent environment, can provide an efficient intermediate-level approach, bridging the gap between microscopic and macroscopic schemes. As an example, we consider an elastic network prototype of a molecular machine [11] and take the solvent into account by using multiparticle collision (MPC) dynamics [13]. Our numerical simulations demonstrate that, within this framework, machine dynamics can be followed for many operation cycles, so a statistical analysis is possible.

The elastic network machine prototype consists of two relatively rigid domains connected by a more flexible joint. This structure mimics that of naturally occurring proteins characterized by large scale hinge motions [14]. It was designed by an optimization procedure to have a relaxation spectrum that is qualitatively similar to that of real hinged proteins, with one small relaxation eigenvalue, related to the hinge motion, which is well separated from other eigenvalues [11]. The special property of the network is that it has a unique attractive conformational relaxation trajectory leading to the equilibrium state. Starting even with large initial deformations, the network rapidly approaches this trajectory and a subsequent slow relation proceeds along it. The potential energy of the network has the form

$$V_n(\mathbf{R}) = \sum_{v=1}^{n_L} \frac{1}{2} k (R_v - R_v^o)^2.$$

The sum is over all bonds in the network, k is the common force constant, R_v is the distance between beads in bond v, R_v^o is the equilibrium bond distance of this bond, and n_L is the number of links. Here $\mathbf{R}$ is the set of all coordinates of the $N_p=64$ beads in the network. The specification of the network can be found in [11].

The network undergoes cyclic conformational changes between open and closed forms, which are coupled to ligand binding and product release. The ligand is attached by connecting it to three special ligand binding beads in an active

*andrew.cressman@utoronto.ca
†togashi@phys1.med.osaka-u.ac.jp
‡mikhailov@fhi-berlin.mpg.de
§rkapral@chem.utoronto.ca

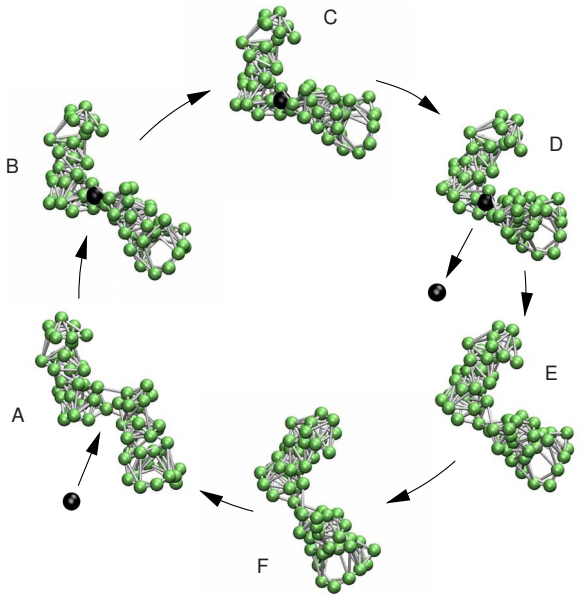

FIG. 1. (Color online) Conformational changes in the elastic network from open O (A) to closed C (D) forms in a machine cycle.

site of the hinge region of the network. The active site is defined by the center of mass of the three beads, and the connections are made through stretched bonds. When the network is in its open state and each of the three bond lengths in the active site lie within $\pm b$ of their open state equilibrium average values, then a ligand may bind with probability p_b. The ligand is chosen to be the nearest solvent molecule, modeling the situation where the ligand concentration is high and ligand binding is not diffusion limited. Ligand-network bonds are formed upon ligand attachment. The network then undergoes a conformational change in order to relieve the resulting tension, bending by approximately 90°. During this transition, the ligand is converted to a product particle that is ready to leave the network. Release of the product occurs from the closed state and, again, if the three bonds in the active site lie within $\pm d$ of their new equilibrium values, release occurs with probability p_d. When the product is released the bonds holding it in place are severed; the network relaxes back to its open state. We consider tight ($b=d=0.04$ and $p_b=p_d=0.0015$) and loose ($b=d=0.05$ and $p_b=p_d=0.0005$) binding-detachment parameters. The cycle is shown in Fig. 1 and a video of the motion is available in [15].

These conformational changes take place in a dense fluctuating molecular environment described by MPC dynamics. In MPC dynamics, N_s solvent particles, representing coarse grained real molecules, free stream and undergo effective collisions at discrete time intervals τ, accounting for the effects of many real collisions during this time interval. The collisions are carried out by dividing the system into a grid of cells $\mathcal{V}_\xi$ and assigning rotation operators $\hat{\omega}_\xi$, chosen from some set of rotation operators, to each cell of the system at the time of collision. Particles within each cell "collide" with each other and the postcollision velocity of particle i in a cell $\mathcal{V}_\xi$ is given by $\mathbf{v}_\mathbf{i}'=\mathbf{V}_\xi+\hat{\omega}_\xi(\mathbf{v}_\mathbf{i}-\mathbf{V}_\xi)$, where $\mathbf{V}_\xi$ is the center of mass velocity of particles in the cell. MPC dynamics satisfies

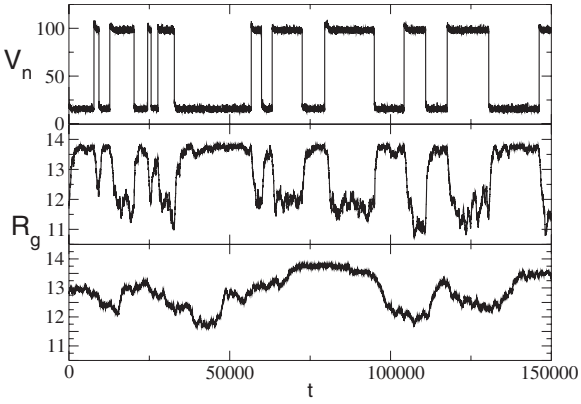

FIG. 2. Cyclic hinge motion with loose binding-detachment parameters. Solvent LJ units, where energy, distance, and mass, $\epsilon=\sigma=m=1$, are used to express system parameters: force constant $k=40$, bead mass $M=10$, number of solvent molecules $N_s=1.08\times10^6$, solvent number density $n_s=5$, $\tau=0.5$, and reduced temperature $k_BT/\epsilon=1/6$ (denoted by T in text). The cubic simulation box had linear dimension $L=60$ and the MPC collision cell size was $a=1$. The molecular dynamics step size was $\Delta t=0.01$. Velocity rotations about a randomly chosen axis by angles $\alpha=\pm\pi/2$. (Top two panels) MPC simulation results for network potential energy, V_n, and radius of gyration, R_g. (Bottom) Simulation without hydrodynamic interactions.

mass, momentum, and energy conservation laws. The dynamics is microcanonical and preserves phase-space volumes [13].

The solvent molecules interact with the network through intermolecular forces, which may be attractive or repulsive, mimicking hydrophilic or hydrophobic interactions. We use repulsive Lennard-Jones (LJ) network-solvent interactions: $V(r)=4\epsilon((\sigma/r)^{12}-(\sigma/r)^6+1/4)$ for $r\leqslant 2^{1/6}$ and zero otherwise. Between MPC events, the system evolves through Newton's equations of motion, taking into account network and network-solvent forces. This hybrid MD-MPC dynamics satisfies all conservation laws [13]. As a result, hydrodynamic interactions are again taken into account. The relative magnitudes of network-solvent and thermal energies are controlled by the reduced temperature T.

The large scale conformational changes between open O and closed C forms of the network that result from the binding and detachment processes can be monitored by observing the radius of gyration of the network, $R_g(\mathbf{R})$, or the angle through which the hinge motion occurs. Figure 2, which plots $V_n(\mathbf{R})$ and $R_g(\mathbf{R})$ versus time, shows the cycling motion of the machine arising from repeated closing and opening due to ligand binding and product detachment. Hydrodynamic interactions can be eliminated by replacing MPC with a random sampling of postcollision velocities from a Boltzmann distribution [16]. Figure 2 (bottom) plots the machine cycle dynamics when hydrodynamic coupling is neglected. The cycle time scale is longer and the dynamics more irregular.

Figure 3 shows four machine cycles in the (V_n,R_g) plane. The temporal direction of the trajectory is indicated by arrows. Binding of a ligand in the O state (A) abruptly increases the elastic energy. This initiates the hinge motion

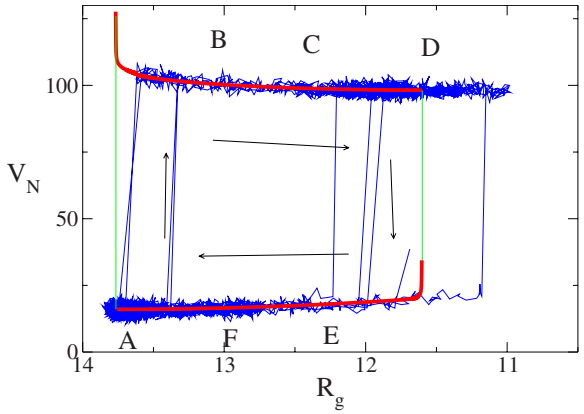

FIG. 3. (Color online) Elastic potential energy V_n versus the radius of gyration R_g for a cyclic trajectory. (Thick line) Deterministic dynamics shifted by the thermal energy. The labels A-F indicate configurations like those in Fig. 3.

(B,C), which represents conformational relaxation toward the *C* state (D). When the ligand is detached, three deformed bonds are removed and the elastic energy falls. Subsequently, reverse conformational hinge motion (E,F) begins, returning the free network to its *O* state. For comparison, Fig. 3 also shows the deterministic trajectories. We see that, in each cycle, hinge motions are regular and closely follow the corresponding deterministic relaxation trajectories for the free network and the ligand-network complex. Transverse fluctuations around the deterministic trajectories are small. There are, however, substantial random variations in the network conformations from which ligand binding and detachment transitions take place. As a result, the durations of the "on" and "off" stages (ligand attached or absent, respectively) fluctuate strongly.

In our mesoscale simulations, tens of machine cycles could be followed, allowing statistical characterization of the cycles and study of their sensitivity to hydrodynamic interactions. Figure 4(a) plots the distribution of cycle times. The cycle time, t_c, is defined as the time interval separating two subsequent ligand binding transitions (sum of the on and off times in a given cycle). Hydrodynamic interactions accelerate conformational relaxation processes. The mean cycle time $\langle t_c \rangle$ decreases from 16 708 to 9185 in the presence of hydrodynamic interactions. The statistical dispersion of t_c is large. The simulated t_c distribution differs from that for a simple stochastic two-state element. To show this, we constructed t_c distributions [black plots in Fig. 4(a)] for an element with just two independent on-off and off-on transitions, each characterized by its own mean waiting time, chosen to be the same as those for the average on and off times in our stochastic machine simulations. The actual distribution is more narrow and the peak is more pronounced than that for the two-state fit. This is because the off-on and on-off transitions are separated by intervals of ordered conformational relaxation motions. Using fluorescent resonant energy transfer and other single-molecule experimental methods, conformational changes and internal rotations in each cycle of molecular machines can be monitored (see, e.g., [17]). For comparison, statistical distributions of the amplitudes of hinge motions in the machine prototype are shown in Fig. 4(b). These amplitudes are defined as the changes of the hinge angle between subsequent off-on and on-off transitions. On average, hydrodynamic interactions increase the amplitude of hinge motions. A more detailed assessment of hydrodynamic effects on the hinge motion can be obtained from the mean first passage times, $t^H_{o\to c}$ and $t^H_{c\to o}$, between *O* and *C* states. Starting from *O* and *C* initial configurations, the times at which a trajectory first crossed the $R_g=12.7$ dividing surface were computed. We find $t^H_{o\to c}=725\pm140$ and $t^H_{c\to o}=569\pm30$ from averages over 40 realizations of the transition processes. The average first passage times without hydrodynamic interactions (free draining) are: $t^{\mathrm{FD}}_{o\to c}=9175\pm1118$ and $t^{\mathrm{FD}}_{c\to o}=6229\pm490$. Since $t^H_{o\to c}/t^{\mathrm{FD}}_{o\to c}=0.08$ and $t^H_{c\to o}/t^{\mathrm{FD}}_{c\to o}=0.09$, including hydrodynamic interactions decreases the closing and opening times by a factor of approximately 10.

From the known value of the kinematic viscosity of the MPC solvent with mass density $\rho_s=mn_s$ [13,18], $\nu=\eta/\rho_s=0.13$, the characteristic length of a domain, $L_d=8$, and the velocity $v=0.004$ of passage between the open and closed states, which can be estimated from the average first passage times and the distance the domains travel, the Reynolds number is found to be $\mathrm{Re}=vL_d/\nu\approx0.25$. Thus, our prototypical molecular machine, like most real molecular machines, operates in the low Reynolds number regime, indicating that inertial effects do not dominate the dynamics.

A phenomenological stochastic description of the network machine dynamics is provided by the many particle Langevin equation [19], $M d\mathbf{V_i}(\mathbf{t})/dt=\mathbf{F}_i(\mathbf{R}(t))-\Sigma_{j=1}^{N_p}\boldsymbol{\zeta}_{ij}(\mathbf{R}(t))\mathbf{V}_j(t)+\mathbf{f}_i(t)$, where $\mathbf{V_i(t)}$ is the velocity of bead *i*, and $\mathbf{F}_i(\mathbf{R})$ and $\mathbf{f}_i$ are the mean force and random force, respectively, on bead *i*. The configuration-dependent friction tensor is $\boldsymbol{\zeta}_{ij}(\mathbf{R})$. Since inertia is not important, the overdamped limit of this equation can be used to model the dynamics. In order to simulate the dynamics using this equation, the spatial dependence of the friction tensor

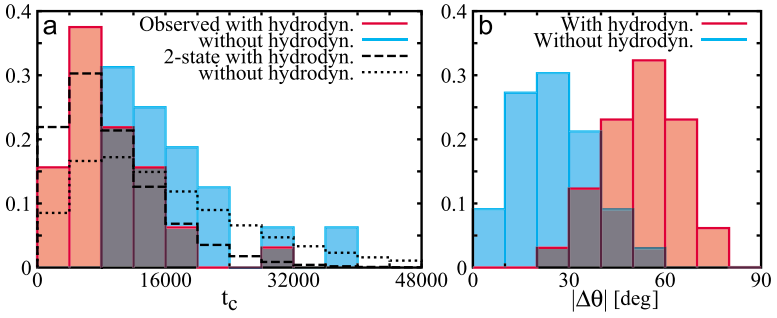

FIG. 4. (Color online) Histograms of cycle times (a) and hinge angle changes (b) for MPC dynamics and dynamics without hydrodynamic interactions, based on data for 32 and 16 cycles, respectively, with tight binding-detachment parameters.

must be specified. The Oseen approximation, $(\boldsymbol{\zeta}(\mathbf{R})^{-1})_{ij}=\zeta_0^{-1}\mathbf{I}\delta_{ij}+\mathbf{T}_{ij}(\mathbf{R}_{ij})$, where the Oseen tensor is $\mathbf{T}_{ij}(\mathbf{R}_{ij})=(1-\delta_{ij})(\mathbf{I}+\hat{\mathbf{R}}_{ij}\hat{\mathbf{R}}_{ij})/(8\pi\eta R_{ij})$, which is derived under the assumption that the beads are separated by distances that are large compared to their size, is often used. Each domain of the network is a nearly rigid object. The effective friction that the center of mass of a domain experiences as a result of the hinge motion is $\boldsymbol{\zeta}_c(\mathbf{R})=\Sigma_{i,j}^{N_d}\boldsymbol{\zeta}_{ij}(\mathbf{R})$, where the sum is over all N_d beads in the domain. If hydrodynamic interactions are ignored, the friction is given by $\boldsymbol{\zeta}_c(\mathbf{R})=N_d\zeta_0\mathbf{I}$. Using a sample configuration of a domain, $\mathbf{R}_d$, the domain friction tensor was computed in the Oseen approximation and it was found that $\boldsymbol{\zeta}_c(\mathbf{R})/N_d\zeta_0\mathbf{I}\approx 0.3$, so that Oseen hydrodynamic interactions reduce the friction by a factor of about 3. Since the domains move to yield open and closed conformational states in response to the forces that arise from the binding and detachment processes, the ratio of the opening-closing times in the presence of hydrodynamic interactions to that without such interactions is $t^H/t^{\mathrm{FD}}\sim\boldsymbol{\zeta}_c(\mathbf{R})/N_d\zeta_0\mathbf{I}$. The change in time scale is not predicted quantitatively; MPC dynamics provides a more accurate description of the hydrodynamic interactions.

Our study of a prototype of molecular machines demonstrated that mesoscale simulations of their operation in fluctuating solvent environments can be carried out. Not only individual operation cycles but also long sequences of such cycles could be followed, enabling statistical analysis. The example considered in our study reveals principal features of the mesoscale approach for modeling molecular machines. While fluctuations are relatively strong, they do not destroy the ordered cyclic dynamics. Except for the rapid transitions that follow after the binding and detachment of a ligand, internal motions of the machine turn out to be well described by a single "mechanical" coordinate, as traditionally assumed in the phenomenological models. Our mesoscopic approach allows one to account for hydrophobic and hydrophilic (not discussed here) interactions with solvent particles and hydrodynamic interactions. The statistical properties of the artificially designed machine prototype agree with the characteristic behavior known for real molecular machines. The method can be extended to simulate elastic models corresponding to actual protein machines, including solvent effects.

The research of R.K. was supported in part by a grant from NSERC Canada and the Alexander von Humboldt Foundation, and that of Y.T. by MEXT, Japan (Yuragi Project).

[1] K. Kinbara and T. Aida, Chem. Rev. (Washington, D.C.) **105**, 1377 (2005).
[2] B. Alberts, Cell **92**, 291 (1998).
[3] P. Ball, Nanotechnology **13**, R15 (2002).
[4] M. Dittrich, J. Yu, and K. Schulten, Top. Curr. Chem. **268**, 319 (2007).
[5] R. D. Astumian, Science **276**, 917 (1997).
[6] F. Jülicher, A. Ajdari, and J. Prost, Rev. Mod. Phys. **69**, 1269 (1997).
[7] M. Doi and S. F. Edwards, *The Theory of Polymer Dynamics* (Clarendon, Oxford, 1986); A. Y. Grosberg and A. R. Khokhlov, *Statistical Physics of Macromolecules* (AIP Press, New York, 1994); N. Gō, Annu. Rev. Biophys. Bioeng. **12**, 183 (1983).
[8] M. M. Tirion, Phys. Rev. Lett. **77**, 1905 (1996); T. Haliloglu, I. Bahar, and B. Erman, *ibid.* **79**, 3090 (1997); F. Piazza, P. De Los Rios, and Y.-H. Sanejouand, *ibid.* **94**, 145502 (2005).
[9] W. Zheng and S. Doniach, Proc. Natl. Acad. Sci. U.S.A. **100**, 13253 (2003); *Normal Mode Analysis: Theory and Applications to Biological and Chemical Systems*, edited by Q. Cui and I. Bahar (CRC Press, Boca Raton, FL, 2006).
[10] O. Miyashita, J. N. Onuchic, and P. G. Wolynes, Proc. Natl. Acad. Sci. U.S.A. **100**, 12570 (2003).
[11] Y. Togashi and A. S. Mikhailov, Proc. Natl. Acad. Sci. U.S.A. **104**, 8697 (2007).
[12] S. O. Nielsen, C. F. Lopez, G. Srinivas, and M. L. Klein, J. Phys.: Condens. Matter **16**, R481 (2004); M. Venturoli, M. M. Sperotto, M. Kranenburg, and B. Smit, Phys. Rep. **437**, 1 (2006).
[13] A. Malevanets and R. Kapral, J. Chem. Phys. **110**, 8605 (1999); **112**, 7260 (2000).
[14] M. Gerstein, A. M. Lesk, and C. Chothia, Biochemistry **33**, 6739 (1994).
[15] See EPAPS Document No. E-PLEEE8-77-R09805 for a video showing cyclic molecular machine operation. For more information on EPAPS, see http://www.aip.org/pubservs/epaps.html.
[16] N. Kikuchi, J. F. Ryder, C. M. Pooley, and J. M. Yeomans, Phys. Rev. E **71**, 061804 (2005).
[17] T. Ha *et al.*, Proc. Natl. Acad. Sci. U.S.A. **96**, 9077 (1999); H. Noji *et al.*, Nature (London) **386**, 299 (1997); Y. Komori, A. H. Iwane, and T. Yanagida, Nat. Struct. Mol. Biol. **14**, 968 (2007).
[18] T. Ihle, E. Tüzel, and D. M. Kroll, Phys. Rev. E **72**, 046707 (2005); C. M. Pooley and J. M. Yeomans, J. Phys. Chem. B **109**, 6505 (2005).
[19] J. M. Deutch and I. Oppenheim, J. Chem. Phys. **54**, 3547 (1971).